

# Quantum spin solver near saturation: QS<sup>3</sup>

Hiroshi Ueda<sup>a,b,c,\*</sup>, Seiji Yunoki<sup>c,d,e,f</sup>, Tokuro Shimokawa<sup>g</sup>

<sup>a</sup>Center for Quantum Information and Quantum Biology, Osaka University, Toyonaka, 560-0043, Japan.

<sup>b</sup>JST, PRESTO, Kawaguchi, 332-0012, Japan

<sup>c</sup>Computational Materials Science Research Team, RIKEN Center for Computational Science (R-CCS), Kobe, 650-0047, Japan

<sup>d</sup>Computational Condensed Matter Physics Laboratory, RIKEN Cluster for Pioneering Research (CPR), Wako, 351-0198, Japan

<sup>e</sup>Computational Quantum Matter Research Team, RIKEN Center for Emergent Matter Science (CEMS), Wako, 351-0198, Japan

<sup>f</sup>Quantum Computational Science Research Team, RIKEN Center for Quantum Computing (RQC), Wako, 351-0198, Japan

<sup>g</sup>Theory of Quantum Matter Unit, Okinawa Institute of Science and Technology Graduate University, Onna, 904-0495, Japan

## Abstract

We develop a program package named QS<sup>3</sup> [kjú:és-kjú:b] based on the (thick-restart) Lanczos method for analyzing spin-1/2 XXZ-type quantum spin models on spatially uniform/non-uniform lattices near fully polarized states, which can be mapped to dilute hardcore Bose systems. All calculations in QS<sup>3</sup>, including eigenvalue problems, expectation values for one/two-point spin operators, and static/dynamical spin structure factors, are performed in the symmetry-adapted bases specified by the number  $N_{\downarrow}$  of down spins and the wave number  $k$  associated with the translational symmetry without using the bit representation for specifying spin configurations. Because of these treatments, QS<sup>3</sup> can support large-scale quantum systems containing more than 1000 sites with dilute  $N_{\downarrow}$ . We show the benchmark results of QS<sup>3</sup> for the low-energy excitation dispersion of the isotropic Heisenberg model on the  $10 \times 10 \times 10$  cubic lattice, the static and dynamical spin structure factors of the isotropic Heisenberg model on the  $10 \times 10$  square lattice, and the open-MP parallelization efficiency on the supercomputer (Ohtaka) based on AMD Epyc 7702 installed at the Institute for the Solid State Physics (ISSP). Theoretical backgrounds and the user interface of QS<sup>3</sup> are also described.

**Keywords:** Exact diagonalization, Lanczos method, Quantum spin system, Dilute hardcore Bose system, Magnetism, Dynamical structure factor

## PROGRAM SUMMARY/NEW VERSION PROGRAM SUMMARY

*Program Title:* QS<sup>3</sup>

*CPC Library link to program files:* (to be added by Technical Editor)

*Developer's repository link:* (if available)

*Code Ocean capsule:* (to be added by Technical Editor)

*Licensing provisions:* MIT

*Programming language:* Fortran90

*External routines/libraries:* BLAS, LAPACK

*Nature of problem:* Physical properties (such as total energy, magnetic moment, two-point spin correlation function, and dynamical structure factor)

*Solution method:* Application software based on the full diagonalization method and the exact diagonalization method using the Lanczos and thick-restart Lanczos techniques for quantum spin  $S = 1/2$  models such as the XXZ model.

*Restrictions:* Spin  $S = 1/2$  systems with U(1) symmetry.

*Unusual features:* Massively large quantum spin systems with U(1) symmetry near the saturation field can be solved with or without considering translational symmetry, which is difficult to treat using standard exact diagonalization libraries with the bit representation for specifying spin configurations.

## 1. Introduction

The exact diagonalization (ED) method [1] is a traditional approach and indeed one of the most powerful numerical methods to correctly understand the nature of quantum many-body systems from finite-size cluster calculations. This method enables us to obtain directly our target eigenvectors and the corresponding eigenvalues of Hamiltonian  $\hat{H}$  and to evaluate all of the static, dynamical, and thermal properties without any bias by storing in physical memory of computers several vectors of the size as large as the dimension of the Hamiltonian matrix. Moreover, in contrast to a quantum Monte Carlo method, which in general suffers from the so-called negative sign problem for fermion and quantum frustrated spin systems, the ED method does not have such kind of difficulty. Therefore, the ED method has been used at the forefront in the research field of quantum many-body systems.

The only disadvantage of the ED method is that the accessible system size is severely limited to small clusters. A direct way to alleviate this disadvantage is to introduce the message-passing-interface (MPI) parallelization [2] and adapt the Hamiltonian symmetry [3]. For examples, sophisticated ED program packages such as SpinPack [4], Rokko [5], and  $\mathcal{H}\Phi$  [6] are designed with MPI techniques for high performance on large-scale supercomputers and use U(1) and/or lattice symmetry to blockdiagonalize the Hamiltonian matrix. Indeed, these large-scale computations with ingenious ways have led to new find-

\*Corresponding author.

E-mail address: h.ueda@qiqb.osaka-u.ac.jp

ings and many discoveries in the long history of studies in the quantum many-body systems, some of which can be found, e.g., in Refs. [7, 8, 9, 10, 11, 12, 13, 14, 15, 16].

Nonetheless, the accessible system sizes are still small because the required computational resources increase exponentially with the system size. For example, for a spin  $S=1/2$  Heisenberg model without magnetic field, the conventional Lanczos algorithm [17] can treat up to 50 spins by fully using the power of a large modern supercomputer [18]. In some particular cases, the system size limitation to small clusters may not be an issue, e.g., in strong random systems [19, 20, 21, 22, 23, 24] and in the high-temperature limit, where the typical correlation lengths are usually small. However, the accessible system size becomes crucial when, for example, gapless or incommensurate phases are discussed in various intriguing quantum many-body systems.

Let us now remind a distinct advantage of the U(1) symmetry adaption for a quantum many-body system that can be mapped to a dilute particle system with a conserved number of particles, e.g., an  $S = 1/2$  XXZ model near the saturation field. In such a system, the ED method can treat much larger system sizes with  $10^3$  sites and more, in principle, because the required matrix dimension is scaled as  $O(N^{\downarrow})$ , instead of  $O(\exp(N))$ , where  $N$  is the system size and  $N_{\downarrow}$  is the number of particles. A protocol in previous ED program packages [4, 6, 25, 26, 27] is to use a bitwise operation and thus the power of the U(1) symmetry is not fully exploited. While the bitwise operation is essential to speedup higher-level arithmetic operations, it requires that all basis states for expressing the Hamiltonian matrix are represented as binary numbers. Therefore, we cannot express the basis for more than 63 sites [28] in a single binary number, e.g., when an  $S = 1/2$  spin model is treated on 64-bit processors.

In this paper, we develop an ED program package named QS<sup>3</sup> (Quantum Spin Solver near Saturation). This package can treat  $S=1/2$  XXZ spin models near the saturation field where the U(1) symmetry is preserved with small  $N_{\downarrow} = O(1)$ . This is the first symmetry adapted open source ED package developed without using the bit representation. QS<sup>3</sup> also adapts the lattice symmetry of the Hamiltonian and thus it is able to treat  $O(10^3)$  sites near the saturation field. A prototype of QS<sup>3</sup> has been already used for analyzing the ground state phase diagram of  $S=1/2$  XXZ spin models on the triangular lattice near the saturation field with system sizes up to 1296 sites [29].

The QS<sup>3</sup> code is based on the Lanczos and thick-restart Lanczos methods [30, 31] to calculate the low-energy eigenvalues and the corresponding eigenvectors of the Hamiltonian matrix, and is supported by the external libraries BLAS and LAPACK [32]. Available physical quantities are the local magnetization, two-point correlation functions, static spin structure factors, and dynamical spin structure factors. For the calculation of the dynamical spin structure factors, the continuous fractional expansion is employed with the Lanczos method [1, 33, 34].

The QS<sup>3</sup> code is specialized to the analysis for quantum magnets under a high magnetic field, dilute hard-core Bose gases, and low-energy properties of ferromagnets. Thus, it is particularly beneficial, for example, to the study of a field-induced spin nematic state [35, 36, 37, 38, 39, 40, 41, 42, 43, 44, 45], which

often emerges in a high magnetic field. The QS<sup>3</sup> code can also be used to estimate magnetic couplings of effective spin Hamiltonians for some materials by directly comparing the spin excitations calculated numerically and measured experimentally by inelastic neutron scattering in a sufficiently high magnetic field. Therefore, the QS<sup>3</sup> package is useful for both theoretical and experimental researchers. The QS<sup>3</sup> package is designed to be executed on generally available computing resources such as laptops and small workstations, and therefore only OpenMP is used for parallelizations. The QS<sup>3</sup> package provides several samples for demonstration calculating physical quantities of  $S=1/2$  XXZ models on three different lattices, the square, triangular, and cubic lattices, which preserve the translational symmetry. The QS<sup>3</sup> package also supports the analysis for systems without the translational symmetry.

The rest of this paper is organized as follows. The basic usage of the QS<sup>3</sup> package is first described in Sec. 2. The algorithms implemented in QS<sup>3</sup> are then explained in Sec. 3. In Sec. 4, benchmark results on the square and cubic lattices are provided, and the bottlenecks and characteristics of the QS<sup>3</sup> calculations are discussed. Finally, the paper is summarized with brief discussion of future extension of the QS<sup>3</sup> package in Sec. 5.

## 2. Basic usage of QS<sup>3</sup>

### 2.1. How to download and build QS<sup>3</sup>

The QS<sup>3</sup> package, containing the Fortran source codes, samples, and manual, is available on GitHub (<https://github.com/QS-Cube/ED>). For building QS<sup>3</sup>, Fortran compiler with BLAS/LAPACK library [32] is prerequisite.

For those who have their own Git accounts, simply clone the repository on their local computers:

```
$ git clone https://github.com/QS-Cube/ED.git
```

Otherwise, go to the web page and click the ‘‘Code’’ button and ‘‘Download ZIP’’ to get ‘‘ED-main.zip’’. The zip file is unpacked as

```
$ unzip ED-main.zip
$ cd ED-main
```

A simple Makefile is provided to build the executable files ‘‘QS3.exe’’ for systems preserving the translational symmetry and ‘‘QS3\_only\_u1.exe’’ for systems without the translational symmetry. The following procedures after the cloning or downloading will generate the executable file and execute sample programs

```
$ cd script
$ ./make.sh
```

After executing samples, each result is stored in the separate directory, ‘‘output\_ex1’’, ‘‘output\_ex2’’,  $\dots$ , and ‘‘output\_ex5’’.

## 2.2. Model

The QS<sup>3</sup> package can treat the following  $S=1/2$  XXZ-type spin Hamiltonian:

$$\hat{\mathcal{H}} = \sum_{r < r'} \{ J_{r,r'}^{xy} (\hat{s}_r^x \hat{s}_{r'}^x + \hat{s}_r^y \hat{s}_{r'}^y) + J_{r,r'}^z \hat{s}_r^z \hat{s}_{r'}^z \} - h^z \sum_{r=1}^N \hat{s}_r^z, \quad (1)$$

where  $\hat{s}_r = (\hat{s}_r^x, \hat{s}_r^y, \hat{s}_r^z)$  is a spin  $S = 1/2$  operator at site  $r$  on an  $N$ -site cluster,  $J_{r,r'}^{z(xy)}$  is the  $z(xy)$  component of the two-body exchange interaction between the  $r$ th and  $r'$ th spins, and  $h^z$  is the uniform magnetic field applied along the  $z$  direction. Since the Hamiltonian  $\hat{\mathcal{H}}$  commutes with the  $z$  component of the total spin, i.e.,  $[\hat{\mathcal{H}}, \sum_r \hat{s}_r^z] = 0$ , the U(1) symmetry is preserved. We also assume that the Hamiltonian  $\hat{\mathcal{H}}$  is translationally invariant under periodic boundary conditions. In the QS<sup>3</sup> package, the lattice structures and the range of the exchange interactions can be varied as long as the U(1) and translational symmetries are preserved. The details will be described below.

## 2.3. How to use QS<sup>3</sup>

Here we explain in detail how to use QS<sup>3</sup> by providing a concrete and simple example of the  $S = 1/2$  isotropic Heisenberg model, i.e.,  $J_{r,r'}^{xy} = J_{r,r'}^z = J_1$  when sites  $r$  and  $r'$  are nearest neighbored and  $J_{r,r'}^{xy} = J_{r,r'}^z = 0$  otherwise, on the  $6 \times 6$  square lattice shown in Fig. 1(a). We calculate the 10 lowest eigenvalues and the corresponding eigenvectors in the subspace of  $\langle \sum_r \hat{s}_r^z \rangle = 15$  and momentum  $\mathbf{k} = (k_x, k_y) = (0, 0)$  by using the thick-restart Lanczos algorithm. Here,  $\langle \sum_r \hat{s}_r^z \rangle$  is the expectation value of the  $z$  component of the total spin with respect to an eigenvector. We also calculate the local magnetization and the two-point correlation function from the obtained eigenvectors, and the dynamical spin structure factor  $S^+(\mathbf{q}, \omega)$  at wave vector  $\mathbf{q} = (q_x, q_y) = (0, 0)$  by means of the continued fraction method.

### 2.3.1. Set a main input file

One should first create several input files in the “input\_ex1” directory. A concrete example of the main input file, input.dat, for the  $S=1/2$  isotropic Heisenberg model on the  $6 \times 6$  square lattice is shown below.

```
&input_parameters
NOS = 36,
NOD = 3,
LX = 6,
LY = 6,
LZ = 1,
KX = 0,
KY = 0,
KZ = 0,
NOxxz = 72,
ALG = 2,
cal_lm = 1,
cal_cf = 1,
cal_dsf = 1,
wr_wf = 1,
re_wf = 0,
```

```
FILExxz = “input_ex1/list_xxz_term_36.dat”,
FILEwf = “work/”,
OUTDIR = “output_ex1/”,
&end
&input_static
NOV = 2,
NOLM = 36,
NOCF = 1296,
FILElm = “input_ex1/list_local_mag.dat”,
FILECF = “input_ex1/list_cf_ss.dat”,
&end
&input_dynamic
spsmsz = 1,
itr_dsf = 200,
QX = 0.0d0,
QY = 0.0d0,
QZ = 0.0d0,
rfield = 0.495d0,
FILEpos = “input_ex1/list_site_position_36_type1.dat”,
&end
&input_lancz
lnc_ene_conv0 = 1.0d-14,
minitr = 20,
maxitr = 10000,
itrinit = 5,
&end
&input_TRLan
NOE = 10,
NOK = 15,
NOM = 30,
maxitr = 10000,
lnc_ene_conv = 1.0d-14,
i_vec_min = 1,
i_vec_max = 1,
&end
```

The main input file given above consists of five parts, input\_parameters, input\_static, input\_dynamic, input\_lancz, and input\_TRLan. The meaning of each part and the variables used there are explained below.

#### input\_parameters

This part requires the users to set fundamental conditions, number of spins, number of down spins, linear dimensions of the cluster, momentum sector, location of the input file specifying the lattice structure and the exchange interactions, locations of outputs for the results, and an algorithm for the calculation of eigenvalues/eigenvectors. The details of the variables are explained below.

**NOS** (INTEGER): Number  $N$  of spins.

**NOD** (INTEGER): Number  $N_d$  of down spins. The users can select the  $z$  component of the total spin,  $M = (N/2 - N_d)$ , by adjusting this valuable.

**LX, LY, LZ** (INTEGER): Linear dimensions  $L_x, L_y,$  and  $L_z$  of the cluster in the  $x, y,$  and  $z$  directions.

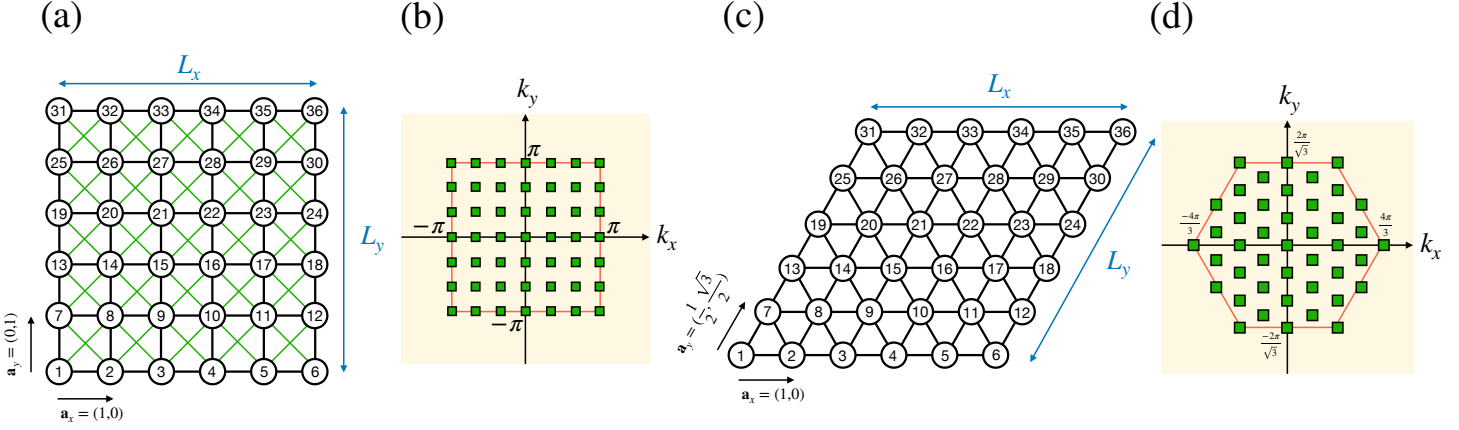


Figure 1: Examples of lattice structures and the corresponding momentum spaces. (a, b) The  $6 \times 6$  square lattice cluster and (c, d) the  $6 \times 6$  triangular lattice cluster. The numbers in each circle in (a) and (c) denote site numbers used in the input file.  $\mathbf{a}_x$  and  $\mathbf{a}_y$  represent the primitive translational vectors, where the lattice constant is set to be one.  $L_x$  ( $L_y$ ) is the linear dimension of the lattice along the  $\mathbf{a}_x$  ( $\mathbf{a}_y$ ) direction (in these examples,  $L_x = L_y = 6$ ). In (b) and (d), the red lines indicate the first Brillouin Zone, and the green squares represent the allowed momentum points,  $\mathbf{k} = (k_x, k_y)$ , for the clusters in (a) and (c), respectively, under periodic boundary conditions. The QS<sup>3</sup> package can compute eigenvalues and eigenvectors of the Hamiltonian matrix at each momentum sector, separately. These momentum points correspond to wave vector points,  $\mathbf{q} = (q_x, q_y)$ , which can be chosen for computing the dynamical spin structure factor  $\mathbf{S}(\mathbf{q}, \omega)$ .

**KX, KY, KZ** (INTEGER): Momentum sector  $K_x$ ,  $K_y$ , and  $K_z$ . The users should set a allowed momentum value that is compatible with the cluster size and shape,  $\mathbf{k} \cdot \mathbf{a}_\alpha = 2\pi K_\alpha / L_\alpha$  with  $\alpha \in \{x, y, z\}$ , where  $\mathbf{k}$  is the momentum and  $\mathbf{a}_\alpha$  is the  $\alpha$  component of the primitive translation vectors.

**NO<sub>xxz</sub>** (INTEGER): Number  $N_{\text{xxz}}$  of the two-body exchange interactions.

**ALG** (INTEGER): The users can choose algorithms by setting 1: Conventional Lanczos, 2: Thick-restart Lanczos, 3: Full diagonalization.

**cal<sub>lm</sub>, cal<sub>cf</sub>, cal<sub>dsf</sub>** (INTEGER): The local magnetization (lm), spin correlation function (cf), and dynamical structure factor (dsf) are calculated by setting the corresponding variables to 1. Otherwise, these variables should be 0.

**wr<sub>wf</sub>** (INTEGER): If  $\text{wr\_wf} = 1$ , the computed eigenvectors are output in the directory specified by FILE<sub>wf</sub>.

**re<sub>wf</sub>** (INTEGER): If  $\text{re\_wf} = 0$ , the whole diagonalization calculation starts from a random initial vector. If  $\text{re\_wf} = 1$ , only the expectation values of physical quantities are computed after reading the eigenvectors already prepared in the directory specified by FILE<sub>wf</sub>.

**FILE<sub>xxx</sub>** (CHARACTER): The location of the file that defines the lattice structure and the two-body exchange interactions  $J_{r,r'}^z$  and  $J_{r,r'}^{xy}$ . The lattice structure is specified in terms of pairs of sites connected by the nonzero interactions. The details are described below.

**FILE<sub>wf</sub>** (CHARACTER): The location of output for the computed eigenvectors. The number of eigenvectors is specified by NOE (the number of the lowest eigenvalues/eigenvectors calculated by an eigensolver specified by ALG).

**OUTDIR** (CHARACTER): The location of output for the computed expectation values such as the local magneti-

zation, spin correlation function, and dynamical structure factor.

#### input\_static

This part requires the users to set the conditions for the calculation of the static physical quantities, i.e., the local magnetization and two-point correlation function. The users should prepare separately the two files that specify the sites and the pairs of sites for the calculation of the local magnetization and the two-point correlation function, respectively.

**NOV** (INTEGER): Number of the lowest eigenvectors used for computing static physical quantities.

**NOLM** (INTEGER): Number of sites for which the local magnetization is computed. If  $\text{NOLM}=0$ , the local magnetization is not computed.

**NOCF** (INTEGER): Number of pairs of sites for which the two-point correlation function is computed. If  $\text{NOCF}=0$ , the correlation function is not computed.

**FILE<sub>lm</sub>** (CHARACTER): The location of the file specifying the site definition of the cluster for the calculation of the local magnetization. The details of the file are explained below.

**FILE<sub>cf</sub>** (CHARACTER): The location of the file specifying the pairs of sites for the calculation of the two-point correlation function. The details of the file are explained below.

#### input\_dynamic

This part requires the users to set the conditions for the calculation of the dynamical spin structure factor. The user should prepare the file specifying the sites of the

cluster, separately.

**spsmsz** (INTEGER):  $S^+(\mathbf{q}, \omega)$ ,  $S^-(\mathbf{q}, \omega)$ , and  $S^z(\mathbf{q}, \omega)$  are computed by setting the value `spsmsz` = 1, 2, and 3, respectively. If `spsmsz` = 0, the dynamical spin structure factor is not computed.

**itr\_dsf** (INTEGER): Number of iterations for the continued fraction method. See Sec. 3.9 for the details.

**QX,QY,QZ** (REAL8): Wave vector point  $\mathbf{q}$  at which the dynamical spin structure factor is computed,  $\mathbf{q} \cdot \mathbf{a}_\alpha = Q_\alpha$ .

**rfield** (REAL8): Magnetic field value  $h_z$ .

**FILEpos** (CHARACTER): The location of the file specifying the site positions. The details of the file are explained below.

#### input\_lancz

This part requires the users to set the conditions for the conventional Lanczos algorithm when the users set `ALG` = 1. The users must set `NOE` = 1 below because only the lowest eigenvalue with the corresponding eigenvector is computed here.

**inc\_ene\_conv0** (REAL8): Convergence condition for the Lanczos iteration.

**min(max)itr** (INTEGER): The minimum/maximum number of iterations for the Lanczos method.

**itrint** (INTEGER): Every `itrint` iterations, the convergence of the Lanczos iteration is checked.

#### input\_TRLan

This part requires the users to set the conditions for the thick-restart Lanczos algorithm when the users set `ALG` = 2.

**NOE** (INTEGER): Number of the lowest eigenvalues/eigenvectors computed by the thick-restart Lanczos method.

**NOK** (INTEGER):  $N_K$  value. See Algorithm 10.

**NOM** (INTEGER):  $N_M$  value. See Algorithm 10.

**maxitr** (INTEGER):  $I_M$  value. See Algorithm 10. The maximum number of iterations for the thick-restart Lanczos method.

**inc\_ene\_conv** (REAL8): Convergence condition for the thick-restart Lanczos iteration.

**i\_vec\_min/max** (INTEGER): Store the `i_vec_min`-th to `i_vec_max`-th lowest eigenvectors computed by the thick-restart Lanczos method in the location specified by `FILEwf`.

#### 2.3.2. Set a file specifying the model

The users are required to specify the lattice structure and the exchange interactions in an input file. We provide in the input directory an example, `list_xxz_term_36.dat`, for the  $S=1/2$

isotropic Heisenberg model on the  $6 \times 6$  square lattice. The file location should be specified in the main input file using the `FILExxz` variable. The first part of `list_xxz_term_36.dat` are shown below.

```
1 2 -1.0E+00 -1.0E+00
2 3 -1.0E+00 -1.0E+00
3 4 -1.0E+00 -1.0E+00
4 5 -1.0E+00 -1.0E+00
```

....

In this data statement, the first and second columns denote the pair of sites ( $r$  and  $r'$ ), and the third and fourth columns represent the corresponding exchange interactions,  $J_{r,r'}^{xy}$  and  $J_{r,r'}^z$ , respectively [see Fig. 1].

#### 2.3.3. Set files for computing physical quantities

The users are required to set several input files for the calculation of physical quantities. For the local magnetization  $\langle \hat{s}_r^z \rangle$ , the users have to specify the site  $r$  for which the local magnetization is computed. For the two-point correlation function  $\langle \hat{s}_r^+ \hat{s}_{r'}^- \rangle$  and  $\langle \hat{s}_r^z \hat{s}_{r'}^z \rangle$ , the users have to specify the pair of sites ( $r, r'$ ) for which the correlation function is computed. As concrete examples, we provide two files in the input directory, `list_local_mag.dat` and `list_cf_ss.dat`, for the local magnetization and the two-point correlation function, respectively.

For the dynamical spin structure factor, the users are required to specify the site positions in the cluster. We also provide an example input file, `list_site_position_36_type1.dat`. Note that the lattice constant is set to be one [see Fig. 1(a)]. The location of these files is specified using `FILExxz`, `FILElm`, and `FILECF` variables in the main input file.

#### 2.3.4. Run and results

After preparing all these files described above, the users can perform the calculation as follows:

```
$. /QS3.exe < input_ex1/input.dat >> output_ex1/output.dat
2>&1
```

Here, `output.dat` is the result file for the calculation, from which the users can check the status of the calculation. The computed results of the physical quantities are output in the directory specified by the `OUTDIR` variable in the main input file. The eigenvectors are output in the directory specified by the `FILEwf` variable in the main input file.

## 3. Implemented algorithms

### 3.1. Representation of states with the $U(1)$ symmetry

The `QS3` package diagonalizes the Hamiltonian matrix for  $\hat{\mathcal{H}}$  given in Eq. (1), consisting of  $N$  spins that can be as large as  $O(10^3)$ , with a small number  $N_\downarrow = O(1) \ll N$  of down spins or equivalently with a large total magnetization value

$M \equiv \langle \phi | \sum_r \hat{s}_r^z | \phi \rangle = N/2 - N_\downarrow$ , where  $|\phi\rangle$  is an eigenstate of  $\hat{\mathcal{H}}$ .

A standard way to construct the spin basis states, and accordingly represent the Hamiltonian matrix, is to use the bit representation, where up ( $\uparrow$ ) and down ( $\downarrow$ ) spins are expressed as 0- and 1-bit values, respectively. However, this is not a practical way for our purpose because a single four-byte (eight-byte) integer can only represent spin basis states up to  $N=31$  (63) [28] in a standard 32 (64)-bit operating system. Furthermore, the definition and operation of arbitrary-byte integers are not supported in standard numerical programming languages.

Let us now explain how to construct the spin basis states in the QS<sup>3</sup> package. We first introduce the following fully polarized state as a vacuum state:

$$|v\rangle \equiv \overbrace{|\uparrow\uparrow\cdots\uparrow\rangle}^{N \text{ spins}}. \quad (2)$$

Each spin basis state  $|a\rangle$  is then constructed by acting the  $S = 1/2$  descending operator  $\hat{s}_r^-$  on the vacuum state, i.e.,

$$|a\rangle = \prod_{m=1}^{N_\downarrow} \hat{s}_{r_m}^- |v\rangle, \quad (3)$$

where  $r_m$  is the position of the  $m$ th down spin in real space. In the QS<sup>3</sup> package, a set of  $\{r_m\}_{1 \leq m \leq N_\downarrow}$  is stored in  $N_\downarrow$ -dimensional integer vector (array)  $\mathbf{n} \equiv (n_1, n_2, \dots, n_{N_\downarrow}) = (r_1, r_2, \dots, r_{N_\downarrow})$  in ascending order,  $1 \leq r_1 < r_2 < \dots < r_{N_\downarrow} \leq N$ , implying that  $r_m \geq m$ .

We now focus on a subspace of the entire Hilbert space of  $\hat{\mathcal{H}}$  by setting the number  $N_\downarrow$  of down spins. The dimension of the subspace is  ${}_N C_{N_\downarrow}$  and the spin basis states  $|a\rangle$  in this subspace are numerated as  $a = 1, 2, \dots, {}_N C_{N_\downarrow}$ . For a given set of  $\{r_m\}_{1 \leq m \leq N_\downarrow}$ , we can define an integer index  $a$  through the following bijective function  $F$ :

$$a = F(\mathbf{n}); F(\mathbf{n}) = 1 + \sum_{m=1}^{N_\downarrow} r_{m-1} C_m. \quad (4)$$

This one-to-one correspondence between  $a$  and  $\{r_m\}_{1 \leq m \leq N_\downarrow}$  can be understood as follows: When the  $N_\downarrow$ th down spin is located at  $r_{N_\downarrow}$ th site, the target spin configuration  $|a\rangle$  should be listed after  ${}_{r_{N_\downarrow}-1} C_{N_\downarrow}$  patterns for arranging  $N_\downarrow$  spins stored within sites from the first site to the  $(r_{N_\downarrow} - 1)$ -th site. We can apply the same procedure for  $m = N_\downarrow - 1$  down to  $m = 1$ , recursively, assuming that  ${}_k C_m = 0$  if  $k < m$ .

The inverse bijective function  $\mathbf{n} = \bar{F}(a)$  is given in Algorithm 1 with the binary search algorithm (Algorithm 2). It is highly instructive to first consider a concrete example. For example, let us consider the case of  $N = 8$ ,  $N_\downarrow = 4$ , and  $\mathbf{n} = (2, 4, 6, 8)$ , which corresponds to  $a = {}_7 C_4 + {}_5 C_3 + {}_3 C_2 + {}_1 C_1 + 1 = 50$ , according to Eq. (4). Now, giving  $s = a = 50$  as the input, we explain how Algorithm 1 outputs  $\mathbf{n} = (2, 4, 6, 8)$ . The algorithm first searches for  $n_4 = r_4 = 8$  that satisfies  ${}_7 C_4 = 35 < s = 50 \leq {}_8 C_4 = 70$  and updates  $s := s - 35 = 15$ .

Second, the algorithm searches for  $n_3 = r_3 = 6$  that satisfies  ${}_5 C_3 = 10 < s = 15 \leq {}_6 C_3 = 20$  and updates  $s := s - 10 = 5$ . Third, the algorithm searches for  $n_2 = r_2 = 4$  that satisfies  ${}_3 C_2 = 3 < s = 5 \leq {}_4 C_2 = 6$  and updates  $s := s - 3 = 2$ . Finally, the algorithm assigns  $n_1 = r_1 = s = 2$ .

More generally, Algorithm 1 first searches for  $n_{N_\downarrow} = r_{N_\downarrow}$  that satisfies  ${}_{r_{N_\downarrow}-1} C_{N_\downarrow} < a \leq {}_{r_{N_\downarrow}} C_{N_\downarrow}$ , followed by a research for  $n_{N_\downarrow-1} = r_{N_\downarrow-1}$  that satisfies  ${}_{r_{N_\downarrow-1}-1} C_{N_\downarrow-1} < a - {}_{r_{N_\downarrow}-1} C_{N_\downarrow} \leq {}_{r_{N_\downarrow-1}} C_{N_\downarrow-1}$ , until a search for  $n_2 = r_2$  that satisfies  ${}_{r_2-1} C_2 < a - \sum_{m=3}^{N_\downarrow} r_{m-1} C_m \leq {}_{r_2} C_2$ . Finally, it uses Eq. (4) to determine  $n_1 = r_1 = a - \sum_{m=2}^{N_\downarrow} r_{m-1} C_m$  and returns  $\mathbf{n}$ . Note that the memory cost with  $O(N_\downarrow N C_{N_\downarrow})$  bytes for keeping the basis sets  $\{\mathbf{n}\}$  in a computer, which may become a memory bottleneck for the Lanczos method, can be reduced to  $O(1)$  by representing the spin basis states with  $|a\rangle$  at the expense of additional numerical cost of  $O(N_\downarrow \ln(N - N_\downarrow))$  for the use of the function  $\bar{F}$ .

---

**Algorithm 1** Generate  $\mathbf{n}$  for given  $a$ .

---

**Input:** integers  $N_\downarrow, N$ , and  $a$  with  $1 \leq a \leq {}_N C_{N_\downarrow}$ .

**Output:**  $N_\downarrow$ -dimensional integer vector  $\mathbf{n}$  with  $1 \leq n_1 < n_2 < \dots < n_{N_\downarrow} \leq N$ .

```

1: function F_BAR( $a, N_\downarrow, N$ )
2:    $s := a$ 
3:    $j := N$ 
4:   for  $m = N_\downarrow$  to 2 with  $m := m - 1$  do
5:      $(j_0, f) = \text{BINARY\_SEARCH}(s - 1, \{ {}_k C_m \}_{1 \leq k \leq j}, m, j)$ 
      $\triangleright$  A logical parameter  $f$  is not used in this function.
      $\triangleright$  Note that  ${}_k C_m = 0$  if  $k < m$ .
6:      $j := j_0$ 
7:      $n_m := j_0 + 1$ 
8:      $s := s - {}_j C_m$ 
9:   end for
10:   $n_1 := s$ 
11:  return ( $\mathbf{n}$ )
12: end function

```

---



---

**Algorithm 2** Check whether  $s_0$  is in  $s$ .

---

**Input:** integer  $s_0, l_s$ , and  $l_e$  ( $\geq l_s$ ), and  $l_e$ -dimensional integer vector  $s$ .

**Output:** integer  $p$  and logical  $f$ .

```

1: function BINARY_SEARCH( $s_0, s, l_s, l_e$ )
2:   Search integer  $p$  in  $\{s_k\}_{l_s \leq k \leq l_e}$  satisfying  $s_p \leq s_0 < s_{p+1}$ 
   with  $l_s \leq p \leq l_e$  by the binary search where  $s_{l_e+1} = \infty$ .
3:    $f := \begin{cases} \text{True} & s_p = s_0 \\ \text{False} & \text{otherwise} \end{cases}$ 
4:   return ( $p, f$ )
5: end function

```

---

### 3.2. Generation of the Hamiltonian matrix

The Hamiltonian matrix is block diagonal with respect to the number  $N_\downarrow$  of down spins and the dimension of the block-diagonal matrix specified with  $(N, N_\downarrow)$  is  ${}_N C_{N_\downarrow}$ . There is a nonzero diagonal contribution of  $\langle a | \hat{s}_r^z \hat{s}_{r'}^z | a \rangle = \pm 1/4$  to the Hamiltonian matrix, where the sign of the value is minus when either  $r$  or  $r'$  is in  $\mathbf{n}$  and otherwise it is plus. For this check, the QS<sup>3</sup> package uses Algorithm 2 of the binary search. On the other hand, the off-diagonal operator  $(\hat{s}_r^+ \hat{s}_{r'}^- + \hat{s}_r^- \hat{s}_{r'}^+)$  acting on a state  $|a\rangle$  can generate a different basis state  $|a'\rangle$  and the corresponding array  $\mathbf{n}' = \bar{F}(a')$ . We can also use the binary search to determine whether a new state is generated. Namely, the new state  $|a'\rangle$  is generated when two logical variables  $f_r$  and  $f_{r'}$ , which are given by  $(p_t, f_t) := \text{BINARY\_SEARCH}(t, \mathbf{n}, 1, N_\downarrow)$  with  $t \in \{r, r'\}$ , are different. If this is the case, the QS<sup>3</sup> package uses Algorithm 3 to make the new array  $\mathbf{n}'$  and we can obtain the off-diagonal matrix element  $\langle a' | \hat{s}_r^+ \hat{s}_{r'}^- + \hat{s}_r^- \hat{s}_{r'}^+ | a \rangle = 1$ . To construct the full matrix elements, we have to consider all sets of  $\{r, r'\}$  compatible with the nonzero exchange interactions in  $\hat{\mathcal{H}}$  given in Eq. (1). For this purpose, the QS<sup>3</sup> package uses Algorithm 4, where the  $N_{\text{xxz}}$  variable is the number of the exchange interactions, i.e., the number of pairs  $\{r, r'\}$  connected via the nonzero exchange interactions, and should be equal to NO<sub>xxz</sub> in the input file. Note that the contribution of the Zeeman term in Eq. (1) is excluded in Algorithm 4 because it is simply constant within the subspace of a fixed  $N_\downarrow$ .

---

#### Algorithm 3 Spin exchange interaction between sites $r$ and $r'$ .

**Input:** integer  $r, p, r' (> r)$ , and  $p' (\geq p)$ ,  $N_\downarrow$ -dimensional integer vector  $\mathbf{n}$ , and logical  $f$ , where  $p, p'$ , and  $f$  are given by  $(p, f) := \text{BINARY\_SEARCH}(r, \mathbf{n}, 1, N_\downarrow)$  and  $(p', f') := \text{BINARY\_SEARCH}(r', \mathbf{n}, 1, N_\downarrow)$ , assuming that  $f' \neq f$ .  
**Output:**  $N_\downarrow$ -dimensional integer vector  $\mathbf{n}'$  with  $1 \leq n'_1 < n'_2 < \dots < n'_{N_\downarrow} \leq N$ .

```

1: function SPIN_EXCHANGE( $r, p, f, r', p', \mathbf{n}$ )
2:   if  $f = \text{False}$  then
3:      $\mathbf{n}' := (n_1, \dots, n_p, r, n_{p+1}, \dots, n_{p'-1}, n_{p'+1}, \dots, n_{N_\downarrow})$ 
4:   else
5:      $\mathbf{n}' := (n_1, \dots, n_{p-1}, n_{p+1}, \dots, n_{p'}, r, n_{p'+1}, \dots, n_{N_\downarrow})$ 
6:   end if
7:   return ( $\mathbf{n}'$ )
8: end function

```

---

### 3.3. Representative states and Hamiltonian matrix elements in symmetry-adapted basis sets

Not only the U(1) symmetry in spin space, but also lattice symmetry such as translational symmetry and point group symmetry can be used to reduce the dimension of the Hamiltonian matrix to be diagonalized and thus the computational cost. Here, we describe how to block-diagonalize the Hamiltonian  $\hat{\mathcal{H}}$  based on the symmetry-adapted basis sets.

---

#### Algorithm 4 Generation of full Hamiltonian matrix.

**Input:**  $N_{\text{xxz}}$ -dimensional integer vectors  $\mathbf{r}$  and  $\mathbf{r}'$ , and  $N_{\text{xxz}}$ -dimensional real vectors  $\mathbf{J}^{\text{xy}}$  and  $\mathbf{J}^z$ .

**Output:**  ${}_N C_{N_\downarrow}$ -dimensional real matrix  $\mathbf{H} = \{h_{a,a'}\}$ .

```

1: function GEN_FULL_HAM( $\mathbf{r}, \mathbf{r}', \mathbf{J}^{\text{xy}}, \mathbf{J}^z$ )
2:    $\mathbf{H} := 0$ 
3:   for  $a = 1$  to  ${}_N C_{N_\downarrow}$  do
4:      $\mathbf{n} := \text{F\_BAR}(a, N_\downarrow, N)$ 
5:     for  $n = 1$  to  $N_{\text{xxz}}$  do
6:        $(p, f) := \text{BINARY\_SEARCH}(r_n, \mathbf{n}, 1, N_\downarrow)$ 
7:        $(p', f') := \text{BINARY\_SEARCH}(r'_n, \mathbf{n}, 1, N_\downarrow)$ 
8:       if  $f = f'$  then
9:          $h_{a,a} := h_{a,a} + \mathbf{J}_n^z/4$ 
10:      else
11:         $h_{a,a} := h_{a,a} - \mathbf{J}_n^z/4$ 
12:         $\mathbf{n}' := \text{SPIN\_EXCHANGE}(r, p, f, r', p', \mathbf{n})$ 
13:         $a' := F(\mathbf{n}')$ 
14:         $h_{a,a'} := \mathbf{J}_n^{\text{xy}}/2$ 
15:      end if
16:    end for
17:  end for
18:  return ( $\mathbf{H}$ )
19: end function

```

---

First, we briefly explain how to construct the symmetry-adapted basis sets that are the eigenstates of the lattice translational operator  $\hat{T}$ . A pedagogical introduction for the construction of the symmetry-adapted basis sets can be found in Ref. [3]. For simplicity, we consider a periodic chain with  $N$  spins, namely  $(L_x, L_y, L_z) = (N, 1, 1)$ , in which the translational operator  $\hat{T}$  is defined by shifting the position of the spin one site right,  $\hat{T}|a\rangle = \prod_{m=1}^{N_\downarrow} \hat{s}_{r_{m+1}}^- |v\rangle$ , with  $\hat{s}_{L+1} = \hat{s}_1$  under periodic boundary conditions. Note that the translational operator  $\hat{T}$  is commutable with the Hamiltonian, i.e.,  $[\hat{T}, \hat{H}] = 0$ , and the accessible eigenvalues of  $\hat{T}$  are given as  $\{e^{ik} \mid k = 2\pi K/N, 0 \leq K < N\}$  with momentum  $k$  or momentum sector  $K$ .

The symmetry-adapted basis states with a given momentum  $k$  is given as

$$|a, k\rangle = \frac{1}{\sqrt{N_{a,k}}} \sum_{j=1}^N e^{-ikj} \hat{T}^j |a\rangle, \quad (5)$$

where  $|a\rangle$  is a single reference state with a fixed number  $N_\downarrow$  of down spins and it is defined in Eq. (3). One can easily confirm that  $|a, k\rangle$  in Eq. (5) is an eigenstate of the translational operator, i.e.,  $\hat{T}|a, k\rangle = e^{ik}|a, k\rangle$ . If the reference state  $|a\rangle$  is not compatible with the momentum  $k$ , the state  $|a, k\rangle$  generated in Eq. (5) vanishes. The compatibility of the chosen reference state  $|a\rangle$  and the normalization factor  $N_{a,k}$  can be determined as

$$N_{a,k} = \frac{N \left| \langle a | \sum_{j=1}^N e^{-ikj} \hat{T}^j | a \rangle \right|^2}{\langle a | \sum_{j=1}^N \hat{T}^j | a \rangle}. \quad (6)$$

If this quantity is zero, it implies that the chosen reference state  $|a\rangle$  is not compatible with the momentum  $k$ . Otherwise, this quantity gives the normalization factor of the state  $|a, k\rangle$ .

Considering the cyclicity of the translated states,  $\{|a_j\rangle \equiv \hat{T}^j|a\rangle\}_{1 \leq j \leq N}$ , we can simply choose only one state as a representative among  $\{|a_j\rangle\}_{1 \leq j \leq N}$ . The QS<sup>3</sup> package chooses one state with the smallest integer  $a$ , i.e.,  $|a\rangle \equiv |\min_j a_j\rangle$ , which is used to generate  $|a, k\rangle$  in Eq. (5). We have to check all possible  ${}_N C_{N_\downarrow}$ -states,  $\{|a\rangle\}$ , in this way, and determine which states and how many states are representatives in the target subspace specified with  $(k, N_\downarrow)$ . The QS<sup>3</sup> package uses Algorithm 5 to check whether or not a state is representative and evaluate the corresponding normalization factor, and uses Algorithm 6 to make a list of the representative states  $\{|a\rangle\}$  and a list of the corresponding normalization factors  $\{N_{a,k}\}$ , representing the symmetry-adapted basis sets  $\{|a, k\rangle\}$ .

---

**Algorithm 5** Check whether a state  $|a\rangle$  is representative, and evaluate the corresponding normalization factor.

---

**Input:** integer  $a$  with  $1 \leq a \leq {}_N C_{N_\downarrow}$ , and real  $k \in$

$\{2\pi K/N\}_{0 \leq K < N}$   
**Output:** real  $N_{a,k} \geq 0$ .

```

1: function CHECK_STATE( $a, k$ )
2:    $\mathbf{n} = \text{F\_BAR}(a, N_\downarrow, N)$ 
3:    $N_{a,k} := 0$ ;  $c^* := 0$ ;  $n_c := 0$ 
4:   for  $j = 1$  to  $N$  do
5:      $\mathbf{n} := \text{SHIFT\_FUNC}(\mathbf{n})$ 
     ▶ The function SHIFT_FUNC( $\mathbf{n}$ ) gives a  $N_\downarrow$ -dimensional
     vector corresponding to a translated state,  $\hat{T}^j|a\rangle$ .
6:      $\mathbf{n} := \text{INSERTION\_SORT}(\mathbf{n})$ 
     ▶ The
     function INSERTION_SORT( $\mathbf{n}$ ) sorts the vector elements in ascending
     order by using the insertion sort algorithm. When  $N_\downarrow$  is  $O(1)$ , we
     confirm that the insertion sort algorithm is generally faster than the
     quick sort algorithm.
7:      $a' := F(\mathbf{n})$ 
8:     if  $a' < a$  then
9:       return ( $N_{a,k} = 0$ )
10:    else
11:      if  $a' = a$  then
12:         $c^* := c^* + e^{ikj}$ ;  $n_c := n_c + 1$ 
13:      end if
14:    end if
15:  end for
16:   $N_{a,k} = |c^*|^2 N / n_c$ 
17:  return ( $N_{a,k}$ )
18: end function

```

---

We are now ready to construct the Hamiltonian matrix based on the symmetry-adapted basis sets  $\{|a, k\rangle\}$ . A state obtained after operating the Hamiltonian  $\hat{\mathcal{H}}$  to each basis state  $|a, k\rangle$  is

---

**Algorithm 6** Making lists of representative states and the corresponding normalization factors.

---

**Input:** real  $k$

**Output:** integer  $d$  with  $0 \leq d \leq {}_N C_{N_\downarrow}$ ,  $d$ -dimensional integer vector  $\sigma$ , and  $d$ -dimensional non-negative real vector  $\mathbf{R}$

```

1: function MK_LIST( $k$ )
2:    $d := 0$ 
3:   for  $a = 1$  to  ${}_N C_{N_\downarrow}$  do
4:      $N_{a,k} := \text{CHECK\_STATE}(a, k)$ 
5:     if  $N_{a,k} > 0$  then
6:        $d := d + 1$ 
7:        $\sigma_d := a$ 
8:        $R_d := \sqrt{N_{a,k}}$ 
9:     end if
10:  end for
11:  return ( $d, \sigma, \mathbf{R}$ )
12: end function

```

---

given by

$$\hat{\mathcal{H}}|a, k\rangle = \frac{1}{\sqrt{N_{a,k}}} \sum_n \sum_{j=1}^N e^{-ikj} \hat{T}^j \hat{h}_n |a\rangle, \quad (7)$$

where

$$\hat{h}_n |a\rangle = \frac{J_n^{xy}}{2} (\hat{s}_{r_n}^+ \hat{s}_{r_n}^- + \hat{s}_{r_n}^- \hat{s}_{r_n}^+) |a\rangle + J_n^z \hat{s}_{r_n}^z \hat{s}_{r_n}^z |a\rangle. \quad (8)$$

Note that the Zeeman term in Eq. (1) can be treated separately because the U(1) symmetry is adapted in the basis sets. We should also note that the off-diagonal term in Eq. (8) flips a spin in the representative state  $|a\rangle$  and the generated state,  $|a^{(n)}\rangle = (\hat{s}_{r_n}^+ \hat{s}_{r_n}^- + \hat{s}_{r_n}^- \hat{s}_{r_n}^+) |a\rangle$ , is not necessarily a representative state. Therefore, we have to check if the flipped state  $|a^{(n)}\rangle$  is compatible with the momentum  $k$ . If it is the case, we have to seek the representative state  $|a^{(n)}\rangle \equiv |\min_j a_j^{(n)}\rangle$  by applying translational operations onto  $|a^{(n)}\rangle$ , i.e.,  $|a_j^{(n)}\rangle \equiv \hat{T}^j |a^{(n)}\rangle$ .

Consequently, we can write Eq. (7) as

$$\begin{aligned} \hat{\mathcal{H}}|a, k\rangle &= \sum_n \frac{J_n^{xy}}{2} e^{-ik\ell_n} \sqrt{\frac{N_{a^{(n)},k}}{N_{a,k}}} (1 - \delta_{f_{n,a}, f'_{n,a}}) |a^{(n)}, k\rangle \\ &+ \sum_n \langle a | J_n^z \hat{s}_{r_n}^z \hat{s}_{r_n}^z | a \rangle |a, k\rangle, \end{aligned} \quad (9)$$

where  $\ell_n$  is obtained from the relationship  $|a^{(n)}\rangle = T^{\ell_n} |a^{(n)}\rangle$  with  $1 \leq \ell_n \leq N$ . The two variables  $f_{n,a}$  and  $f'_{n,a}$  are logical ones given by  $(p_{n,a}, f_{n,a}) := \text{BINARY\_SEARCH}(r_{n,\text{F\_BAR}}(a, N_\downarrow, N), 1, N_\downarrow)$  and  $(p'_{n,a}, f'_{n,a}) := \text{BINARY\_SEARCH}(r'_{n,\text{F\_BAR}}(a, N_\downarrow, N), 1, N_\downarrow)$ , respectively. These variables are used to judge if each off-diagonal term in the Hamiltonian contributes. In the QS<sup>3</sup> package, Algorithm 7 is used to search the representative state  $|a^{(n)}\rangle$  for the off-diagonal matrix elements and to obtain the corresponding  $\ell_n$  value, and Algorithm 8 is to construct the Hamiltonian matrix. Note the order of two for-loops associated with a

and  $n$  in Algorithm 8 that is chosen to enhance the performance of open MP parallelization applying to  $\mathbf{a}$ .

---

**Algorithm 7** Seeking the representative state  $\mathbf{a}^{(n)}$  and the  $\ell_n$  value for operations in Eq. (9)

---

**Input:** integer  $a^{(n)}$  and  $N_\downarrow$   
**Output:** integer  $\mathbf{a}^{(n)}$  and  $\ell_n$ .

- 1: **function** REPRESENTATIVE( $a^{(n)}, N_\downarrow$ )
- 2:    $\mathbf{a}^{(n)} := a^{(n)}$
- 3:    $\mathbf{n} := \text{F\_BAR}(a^{(n)}, N_\downarrow, N)$
- 4:   **for**  $j = 1$  to  $N$  **do**
- 5:      $\mathbf{n} := \text{SHIFT\_FUNC}(\mathbf{n})$
- 6:      $\mathbf{n} := \text{INSERTION\_SORT}(\mathbf{n})$
- 7:      $\mathbf{a} := F(\mathbf{n})$
- 8:     **if**  $\mathbf{a} \leq \mathbf{a}^{(n)}$  **then**
- 9:        $\mathbf{a}^{(n)} := \mathbf{a}; \ell_n := j$
- 10:    **end if**
- 11:   **end for**
- 12:   **return** ( $\mathbf{a}^{(n)}, \ell_n$ )
- 13: **end function**

---

### 3.4. Full diagonalization

One can full diagonalize the whole Hamiltonian to obtain all eigenvalues  $\{E_\nu\}$  and the corresponding eigenvectors  $\{|\nu\rangle\}$  by separately diagonalizing block diagonalized Hamiltonian matrices constructed via Algorithm 4 or Algorithm 8 with different symmetry sectors. Accordingly, one can for example compute the temperature dependence of any physical quantity  $\hat{A}$  based on the thermal average,

$$\langle \hat{A} \rangle_{\beta, N}^{\text{ens}} = \sum_{\nu} \frac{e^{-\beta E_\nu}}{Z(\beta)} \langle \nu | \hat{A} | \nu \rangle, \quad (10)$$

where  $\beta$  is the inverse temperature,  $Z(\beta) = \sum_{\nu} e^{-\beta E_\nu}$  is the partition function, and the summation of  $\nu$  runs over all symmetry sectors with different values of  $N_\downarrow$  and/or  $k$ . However, note that the accessible matrix dimension is very limited in the full diagonalization calculation, typically up to  $O(10^4)$  on a currently available standard computer. Therefore, one may not be able to treat all subspaces of the Hamiltonian even when the Hamiltonian matrix is block diagonalized with different symmetry sectors.

The QS<sup>3</sup> package is specialized for the system under a high magnet field, in which one can treat much larger system sizes near the saturation field. This implies that one may access the finite temperature physics of large systems but at sufficiently low temperature where the low-energy eigenvalues are reasonably separated from those for the symmetry sectors with larger  $N_\downarrow$  and thus the latter contribution to the thermal average  $\langle \hat{A} \rangle_{\beta, N}^{\text{ens}}$  can be simply discarded.

The QS<sup>3</sup> package uses DHEEVR/ZHEEVR routine in LAPACK [32] for the full diagonalization to obtain all eigenvalues and eigenvectors of the Hamiltonian matrix constructed with the symmetry-adapted basis sets.

---

**Algorithm 8** Generation of Hamiltonian matrix with the symmetry-adapted basis sets.

---

**Input:**  $N_{\text{xxz}}$ -dimensional integer vectors  $\mathbf{r}$  and  $\mathbf{r}'$ ,  $N_{\text{xxz}}$ -dimensional real vectors  $\mathbf{J}^{\text{xy}}$  and  $\mathbf{J}^z$ ,  $d$ -dimensional integer vector  $\boldsymbol{\sigma}$  and real vector  $\mathbf{R}$  for the lists of the representative states and their normalization factors, respectively, and real  $k$

**Output:**  $d$ -dimensional complex matrix  $\mathbf{H} = \{h_{\mathbf{a}, \mathbf{a}'}\}$ .

- 1: **function** GEN\_FULL\_HAM\_SYM\_ADAPT( $\mathbf{r}, \mathbf{r}', \mathbf{J}^{\text{xy}}, \mathbf{J}^z, \boldsymbol{\sigma}, \mathbf{R}, k$ )
- 2:    $\mathbf{H} := 0$
- 3:   **for**  $\mathbf{a} = 1$  to  $d$  **do**
- 4:      $\mathbf{n} = \text{F\_BAR}(\sigma_{\mathbf{a}}, N_\downarrow, N)$
- 5:     **for**  $n = 1$  to  $N_{\text{xxz}}$  **do**
- 6:        $(p, f) := \text{BINARY\_SEARCH}(r_n, \mathbf{n}, 1, N_\downarrow)$
- 7:        $(p', f') := \text{BINARY\_SEARCH}(r'_n, \mathbf{n}, 1, N_\downarrow)$
- 8:       **if**  $f = f'$  **then**
- 9:           $h_{\mathbf{a}, \mathbf{a}} := h_{\mathbf{a}, \mathbf{a}} + \mathbf{J}_n^z / 4$
- 10:       **else**
- 11:           $h_{\mathbf{a}, \mathbf{a}} := h_{\mathbf{a}, \mathbf{a}} - \mathbf{J}_n^z / 4$
- 12:           $\mathbf{a}' := F(\text{SPIN\_EXCHANGE}(r, p, f, r', p', \mathbf{n}))$
- 13:           $(\mathbf{a}', \ell) := \text{REPRESENTATIVE}(\mathbf{a}', N_\downarrow)$
- 14:           $(\mathbf{a}', f) := \text{BINARY\_SEARCH}(\mathbf{a}', \boldsymbol{\sigma}, 1, d)$
- 15:          **if**  $f = \text{True}$  **then**
- 16:            $h_{\mathbf{a}, \mathbf{a}'} := h_{\mathbf{a}, \mathbf{a}'} + \frac{\mathbf{J}_n^{\text{xy}}}{2} e^{ik\ell} \sqrt{R_{\mathbf{a}'}/R_{\mathbf{a}}}$
- 17:          **end if**
- 18:       **end if**
- 19:     **end for**
- 20:   **end for**
- 21:   **return** ( $\mathbf{H}$ )
- 22: **end function**

---

### 3.5. Multiplying Hamiltonian to state vectors (matrix-vector product)

In order to calculate the lowest eigenvalue (and also the several lowest eigenvalues) and the corresponding eigenvector(s) of the Hamiltonian matrix, one can also employ the conventional Lanczos method, instead of the full diagonalization, which allows us to treat larger system sizes. The main and most time-consuming part in the Lanczos method is a matrix-vector product, and the QS<sup>3</sup> package does this operation based on the symmetry-adapted basis sets. Assuming that both the U(1) and translational symmetries are adapted, the resulting vector after the matrix-vector product operation  $\hat{H}|\phi\rangle$  is expressed with the basis sets  $\{|\mathbf{a}, k\rangle\}$  and each element  $\psi_{\mathbf{a}, k}$  can be obtained as

$$\begin{aligned} \psi_{\mathbf{a}, k} &= \langle \mathbf{a}, k | \psi \rangle = \langle \mathbf{a}, k | \hat{H} | \phi \rangle \\ &= \sum_n \frac{\mathbf{J}_n^{\text{xy}}}{2} e^{ik\ell_n} \sqrt{\frac{N_{\mathbf{a}^{(n)}, k}}{N_{\mathbf{a}, k}}} (1 - \delta_{f_{n, \mathbf{a}}, f'_{n, \mathbf{a}}}) \phi_{\mathbf{a}^{(n)}, k} \\ &\quad + \sum_n \langle \mathbf{a} | \mathbf{J}_n^z \hat{s}_{r_n}^z \hat{s}_{r'_n}^z | \mathbf{a} \rangle \phi_{\mathbf{a}, k}, \end{aligned} \quad (11)$$

where a state vector  $|\phi\rangle = \sum_{\mathbf{a}} \phi_{\mathbf{a}, k} |\mathbf{a}, k\rangle$  is an input vector. The QS<sup>3</sup> package uses Algorithm 9 to do this procedure. Note that



One can easily show that the operator  $\hat{S}_q^\alpha$  satisfies the following relation:

$$\hat{S}_q^\alpha \hat{T}^j = e^{-iqj} \hat{T}^j \hat{S}_q^\alpha. \quad (15)$$

Using this relation, one of the basic operations,  $\hat{S}_q^\alpha |\phi\rangle$ , necessary for computing the static and dynamical spin structure factors can be rewritten as

$$\hat{S}_q^\alpha |\phi\rangle = \sum_a \phi_{a,k} \hat{S}_q^\alpha |a, k\rangle \quad (16)$$

with

$$\begin{aligned} \hat{S}_q^\alpha |a, k\rangle &= \frac{1}{\sqrt{N_{a,k}}} \sum_j e^{-ikj} \hat{S}_q^\alpha \hat{T}^j |a\rangle \\ &= \frac{1}{\sqrt{N_{a,k}}} \sum_j e^{-i(k+q)j} \hat{T}^j \hat{S}_q^\alpha |a\rangle \\ &= \frac{1}{\sqrt{N_{a,k} N}} \sum_{j,j'} e^{-i(k+q)j} \hat{T}^j e^{-iqj'} \hat{T}^{j'} \hat{S}_1^\alpha (\hat{T}^{j'})^\dagger |a\rangle, \end{aligned} \quad (17)$$

where  $|\phi\rangle = \sum_a \phi_{a,k} |a, k\rangle$  is an eigenvector of the Hamiltonian matrix and it is in the subspace specified with momentum  $k$  and the number  $N_\downarrow$  of down spins. Note that in computing the transverse components of the spin structure factors with  $\alpha = \pm$  in Eq. (17), we have to consider a transition between states with different  $U(1)$  symmetry sectors, i.e., from a state  $|a\rangle$  with  $N_\downarrow$  down spins to a state  $\hat{S}_q^{\alpha\pm} |a\rangle$  with  $N_\downarrow \mp 1$  down spins.

Let us now introduce the spin state  $|b\rangle$  defined as

$$\hat{T}^{j'} \hat{S}_1^\alpha (\hat{T}^{j'})^\dagger |a\rangle = c |b\rangle \quad (18)$$

with  $c = \langle b | \hat{T}^{j'} \hat{S}_1^\alpha (\hat{T}^{j'})^\dagger |a\rangle$ . Note that  $|b\rangle$  as well as  $c$  depends on  $\alpha, j'$ , and  $a$ . In general, the state  $|b\rangle$  is not the representative state  $|b\rangle \equiv |\min_j b_j\rangle$  for states  $\{|b_j\rangle \equiv \hat{T}^j |b\rangle\}_{1 \leq j \leq N}$ , and  $|b\rangle$  can be translated to  $|b\rangle$  by repeatedly applying the translational operator  $\hat{T}$ , i.e.,  $|b\rangle = \hat{T}^\ell |b\rangle$  with  $1 \leq \ell \leq N$ , where  $\ell$  depends on  $|b\rangle$ . Therefore, we can rewrite Eq. (17) using the representative state  $|b\rangle$  as

$$\begin{aligned} \hat{S}_q^\alpha |a, k\rangle &= \frac{1}{\sqrt{N_{a,k} N}} \sum_{j,j'} e^{-i(k+q)j} \hat{T}^j e^{-iqj'} c \hat{T}^{-\ell} |b\rangle \\ &= \frac{1}{\sqrt{N_{a,k} N}} \sum_{j,j'} e^{-i(qj' + (k+q)\ell)} c e^{-i(k+q)(j-\ell)} \hat{T}^{j-\ell} |b\rangle \\ &= \frac{1}{\sqrt{N_{a,k} N}} \sum_j \sqrt{N_{b,k+q}} e^{-i(qj' + (k+q)\ell)} c |b, k+q\rangle. \end{aligned} \quad (19)$$

A concrete procedure for performing  $\hat{S}_q^- |\phi\rangle$  is shown in Algorithm 11. In the same manner, we can perform  $\hat{S}_q^+ |\phi\rangle$  and  $\hat{S}_q^z |\phi\rangle$ .

### 3.9. Continued fraction expansion based on the Lanczos algorithm

Using the continued fraction expansion based on the Lanczos algorithm [1, 33, 34], the QS<sup>3</sup> package computes the dynamical spin structure factor

$$S_q^\alpha(\omega) = -\frac{1}{\pi} \text{Im} \langle \phi | \hat{S}_q^{\alpha\dagger} \frac{1}{\omega - \hat{H} + E_0 + i\eta} \hat{S}_q^\alpha | \phi \rangle, \quad (20)$$

where  $E_0$  is the ground state energy (i.e., lowest eigenvalue) with the corresponding ground state  $|\phi\rangle$  of the Hamiltonian  $\hat{H}$  and positive real number  $\eta$  is the broadening factor. We can rewrite the above equation as

$$S_q^\alpha(\omega) = -\frac{1}{\pi} \text{Im} \frac{\langle \phi | \hat{S}_q^{\alpha\dagger} \hat{S}_q^\alpha | \phi \rangle}{z - \alpha_1 - \frac{\beta_1^2}{z - \alpha_2 - \frac{\beta_2^2}{z - \alpha_3 - \dots}}} \quad (21)$$

with  $z = \omega - E_0 + i\eta$ .  $\alpha$  and  $\beta$  in Eq. (21) are obtained by the tridiagonalization procedure of the Hamiltonian matrix in the Lanczos iteration shown in lines 3-11 of Algorithm 10 with the initial state  $|\psi\rangle_1 = \hat{S}_q^\alpha |\phi\rangle$  that can be prepared by the procedure shown in Algorithm 11.

## 4. Benchmark results

### 4.1. Parallelization efficiency with openMP

Here we show a benchmark result of the QS<sup>3</sup> package for the numerical diagonalization. The most time consuming part in the Lanczos algorithm is the Hamiltonian-vector multiplication in Algorithm 9 with computational complexity  $O(N C_{N_\downarrow} N_{\text{xxx}} N_\downarrow \ln N_\downarrow)$ . The QS<sup>3</sup> package adopts OpenMP to parallelize this procedure. For a typical benchmark, we consider an  $S = 1/2$  isotropic antiferromagnetic Heisenberg model on a simple cubic lattice of 216 sites ( $L_x = L_y = L_z = 6$ ) and calculate the ground state in the subspace with momentum  $\mathbf{k} = (0, 0, 0)$  and  $N_\downarrow = 5$ , by setting the parameters  $(K_x, K_y, K_z) = (0, 0, 0)$ , using the conventional Lanczos algorithm. The dimension of the Hilbert space (i.e., the Hamiltonian matrix) is  ${}_{216}C_5 (=3,739,729,608)$  with only adapting the  $U(1)$  symmetry and can be reduced  $1/N$  times smaller down to 17,313,563 when the translational symmetry is also adapted. Figure 2 shows the efficiency of the parallelization of the QS<sup>3</sup> package executed using the supercomputer (Ohtaka) in ISSP with AMD Epyc 7702 2.0 GHz. We confirm almost linear acceleration with increasing the number of threads up to 128, although the slope becomes somewhat smaller when the number of threads exceeds around 20.

### 4.2. Energy-dispersion relation

One of the essential physical quantities to understand the low-energy physics of a quantum spin model is the energy-dispersion relation  $E_0(\mathbf{k})$ , the ground state energy at each momentum  $\mathbf{k}$ . Most of the currently available exact diagonalization libraries compute this quantity but are sufficient for practical use only in one-dimensional systems because of the severe

---

**Algorithm 10** Thick-restart Lanczos method

---

**Input:** integer  $N_K (> 0)$ ,  $N_M (> N_K)$ ,  $d$ , and  $I_M (> 0)$ , and real  $\epsilon \ll 1$

**Output:** real  $e = \{e_x\}_{1 \leq x \leq N_M}$  and complex  $\Psi = \{\psi_{ax}\}_{1 \leq a \leq d, 1 \leq x \leq N_M}$ .

```
1: function THICK_RESTART_LANCZOS( $N_K, N_M, I_M, \epsilon$ )
2:    $\psi_x = \{\psi_{ax}\}_{1 \leq a \leq d}$ ;  $\psi_1 := \text{RANDOM\_VEC}(d)$ 
    $\triangleright$  The function RANDOM_VEC( $d$ ) returns  $d$ -dimensional
   complex random vector.
3:    $\beta_0 := \sqrt{|\psi_1|^2}$ 
4:   for  $x = 1$  to  $N_M$  do
5:      $\psi_x := \psi_x / \beta_{x-1}$ 
6:      $v := \text{HAM\_TO\_VEC}(r, r', J^{xy}, J^z, \sigma, k, \psi_x)$ 
7:      $\alpha_x := \psi_x^\dagger \cdot v$ 
8:      $\psi_{x+1} := \begin{cases} v - \alpha_x \psi_x & (x = 1) \\ v - \alpha_x \psi_x - \beta_{x-1} \psi_{x-1} & (x > 1) \end{cases}$ 
9:      $\psi_{x+1} := \text{REORTHOGONALIZATION}(\Psi, x + 1)$ 
    $\triangleright$  The function REORTHOGONALIZATION( $\Psi, x$ ) performs
   reorthogonalization, for example, with the modified Gram-
   Schmidt procedure, to numerically keep the orthogonality
    $\psi_{x' < x}^\dagger \cdot \psi_x = 0$ .
10:     $\beta_x := \sqrt{|\psi_{x+1}|^2}$ 
11:  end for
12:   $\psi_{N_{M+1}} := \psi_{N_{M+1}} / \beta_{N_M}$ 
13:   $(e, C = \{c_{x,x'}\}) := \text{DIAG\_TRI}(\{\alpha_x\}, \{\beta_x\})$ 
    $\triangleright$  The function DIAG_TRI( $\{\alpha_x\}, \{\beta_x\}$ ) returns eigenvalues  $e$ 
   (ascending order) and the corresponding eigenvectors  $C$  of
   a real symmetric tridiagonal matrix with diagonal elements
    $\{\alpha_x\}$  and sub-diagonal elements  $\{\beta_x\}$ .
14:  for  $l = 1$  to  $I_M$  do
15:     $\{\psi_y\}_{1 \leq y \leq N_K} := \Psi\{c_{x,y}\}$ 
16:    if  $l = 1$  then
17:       $e' = \{e_y\}_{1 \leq y \leq N_K}$ 
18:    else
19:      if  $\max_{1 \leq y \leq N_K} |e'_y / e_y - 1| < \epsilon$  then
20:        Exit
21:      else
22:         $e' = \{e_y\}_{1 \leq y \leq N_K}$ 
23:      end if
24:    end if
25:     $\{\alpha_y\}_{1 \leq y \leq N_K} := \{e_y\}$ 
26:     $\psi_{N_K+1} := \psi_{N_{M+1}}$ 
27:     $\{\beta_y\}_{1 \leq y \leq N_K} := \{\beta_{N_M} c_{N_M, y}\}$ 
28:    lines 6 and 7 with  $x = N_K + 1$ .
29:     $v := v - \sum_y \beta_y \psi_y$ 
30:     $\psi_{N_K+2} := v - \alpha_{N_K+1} \psi_{N_K+1}$ 
31:     $\psi_{N_K+2} := \text{REORTHOGONALIZATION}(\Psi, N_K + 2)$ 
32:     $\beta_{N_K+1} := \sqrt{|\psi_{N_K+2}|^2}$ 
33:    lines 4-12 with the starting value of  $x = N_K + 2$ .
34:     $\mathbf{T} := 0$ 
35:     $\{t_{xx}\}_{1 \leq x \leq N_M} = \{\alpha_x\}$ 
36:     $\{t_{y, N_K+1}\}_{1 \leq y \leq N_K} = \{t_{N_K+1, y}^*\} := \{\beta_y\}$ 
37:     $\{t_{z, z+1}\}_{N_K+1 \leq z \leq N_M-1} = \{t_{z+1, z}^*\} := \{\beta_z\}$ 
38:     $(e, C) := \text{DIAG}(\mathbf{T})$ 
```

$\triangleright$  The  
function `DIAG( $\mathbf{T}$ )` returns eigenvalues (ascending order) and  
the corresponding eigenvectors of Hermitian matrix  $\mathbf{T}$ .

```
39:  end for
40:  return  $(e, \Psi)$ 
41: end function
```

---

---

**Algorithm 11** Perform  $|\psi'\rangle := \hat{S}_q^{-1}|\phi\rangle$ 

---

**Input:** real  $k$  and  $q \in \{2\pi K/N\}_{0 \leq K < N}$ ,  $d$ -dimensional integer vector  $\sigma$  and real vector  $\mathbf{R}$  for the lists of representative states specified with  $N_\downarrow$  down spins and their normalization factors, respectively,  $d$ -dimensional complex vector  $\phi$ , and  $d'$ -dimensional integer vector  $\sigma'$  and real vector  $\mathbf{R}'$  for the lists of representative states specified with  $N_\downarrow + 1$  down spins and their normalization factors, respectively.

**Output:**  $d'$ -dimensional complex vector  $\psi'$ .

```
1: function SMQ_TO_VEC( $\sigma, \mathbf{R}, k, \phi, \sigma', \mathbf{R}'$ ,  $q$ )
2:    $\psi' := 0$ 
3:   for  $r = 1$  to  $N$  do
4:     for  $a = 1$  to  $d$  do
5:        $n = \text{F\_BAR}(\sigma_a, N_\downarrow, N)$ 
6:        $(p, f) := \text{BINARY\_SEARCH}(r, n, 1, N_\downarrow)$ 
7:       if  $f = \text{False}$  then
8:          $n' := (n_1, \dots, n_p, r, n_{p+1}, \dots, n_{N_\downarrow})$ 
9:          $b := F(n')$ 
10:         $(b, \ell) := \text{REPRESENTATIVE}(b, N'_\downarrow)$ 
11:         $(b, f) := \text{BINARY\_SEARCH}(b, \sigma', 1, d')$ 
12:        if  $f = \text{True}$  then
13:           $\psi'_b := \psi'_b + \sqrt{\frac{R'_b}{R_a N}} e^{-i(qr + (k+q)\ell)} \phi_a$ 
14:        end if
15:      end if
16:    end for
17:  end for
18:  return  $(\psi')$ 
19: end function
```

---

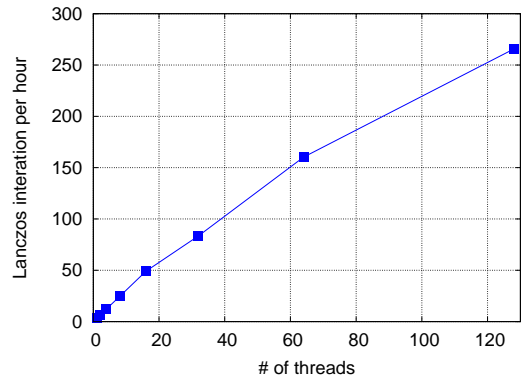


Figure 2: Parallelization efficiency of the QS<sup>3</sup> package. The conventional Lanczos algorithm is used to calculate the ground state of an  $S = 1/2$  isotropic antiferromagnetic Heisenberg model on a simple cubic lattice of 216 sites with  $(K_x, K_y, K_z) = (0, 0, 0)$  and  $N_\downarrow = 5$ .

limitations of the accessible system sizes. The QS<sup>3</sup> package can evaluate the energy-dispersion relation around the saturation field even in three-dimensional systems.

For demonstration, we show the energy-dispersion relation for an  $S = 1/2$  isotropic antiferromagnetic Heisenberg model on a simple cubic lattice of 1000 sites ( $L_x = L_y = L_z = 10$ ) in Fig. 3. When only the U(1) symmetry is used, the dimension of the Hilbert space with  $N_\downarrow = 3$  is  ${}_{1000}C_3 = 166,167,000$  and approximately 2.5 GByte of physical memory is required to store a state vector with the double-complex precision. This implies that the total physical memory up to about 8 GByte is required to obtain the ground state by means of the conventional Lanczos method. This is rather expensive to perform on a standard laptop computer. However, by incorporating the translational symmetry, the required storage per a state vector is reduced down to around 2.5 MByte, and thus the computation can be executed easily with a laptop computer.

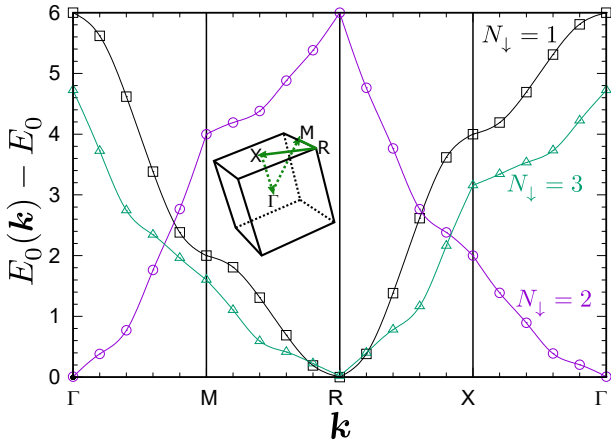


Figure 3: Energy-dispersion relation  $E_0(\mathbf{k})$  of an  $S = 1/2$  isotropic antiferromagnetic Heisenberg model on a simple cubic lattice of 1000 sites ( $L_x = L_y = L_z = 10$ ) with  $N_\downarrow$  down spins along the high symmetric momentum  $\mathbf{k}$  line indicated in the inset. The lowest eigenenergies  $E_0(\mathbf{k})$  with  $N_\downarrow = 1, 2,$  and  $3$  near the saturation field are plotted relative to the ground state energy  $E_0$  of the fully polarized state with  $N_\downarrow = 0$ . The high symmetric momentum points are indicated by  $\Gamma$ :  $(0, 0, 0)$ ,  $M$ :  $(0, \pi, \pi)$ ,  $R$ :  $(\pi, \pi, \pi)$ , and  $X$ :  $(0, 0, \pi)$ . Solid lines are the cubic-spline interpolation in each path, i.e.,  $\Gamma \rightarrow M$ ,  $M \rightarrow R$ ,  $R \rightarrow X$ , and  $X \rightarrow \Gamma$ .

### 4.3. Static and dynamical structure factors

In Fig. 4, we also demonstrate the calculation of the static and dynamical spin structure factors for an  $S = 1/2$  isotropic antiferromagnetic Heisenberg model on a square lattice of 100 sites ( $L_x = L_y = 10$ ) with  $N_\downarrow = 2$ . The static spin structure factor  $S_{\mathbf{q}}^\alpha$  is defined as

$$S_{\mathbf{q}}^\alpha = \langle \phi | \hat{S}_{\mathbf{q}}^{\alpha\dagger} \hat{S}_{\mathbf{q}}^\alpha | \phi \rangle \quad (22)$$

with  $|\phi\rangle$  being the ground state and it is related to the dynamical spin structure factor  $S_{\mathbf{q}}^\alpha(\omega)$  via

$$S_{\mathbf{q}}^\alpha = \int S_{\mathbf{q}}^\alpha(\omega) d\omega. \quad (23)$$

A nearly fully polarized state always displays a trivial but dominant sharp peak in the longitudinal structure factor at the  $\Gamma$  point and the symmetrically equivalent momenta. For ease of visibility, this trivial component is subtracted from the calculated static and dynamical longitudinal spin structure factors, denoted respectively as  $\tilde{S}_{\mathbf{q}}^z$  and  $\tilde{S}_{\mathbf{q}}^z(\omega)$  in Fig. 4. Here, the dynamical spin structure factor  $\tilde{S}_{\mathbf{q}}^z(\omega)$  at  $\mathbf{q} = \mathbf{0}$  is given as

$$\tilde{S}_{\mathbf{q}=\mathbf{0}}^z(\omega) \equiv S_{\mathbf{q}=\mathbf{0}}^z(\omega) - \frac{\eta}{\pi(\omega^2 + \eta^2)} \frac{M^2}{N} \quad (24)$$

and  $\tilde{S}_{\mathbf{q}}^z(\omega)$  at  $\mathbf{q} \neq \mathbf{0}$  is exactly the same as  $S_{\mathbf{q}}^z(\omega)$ .

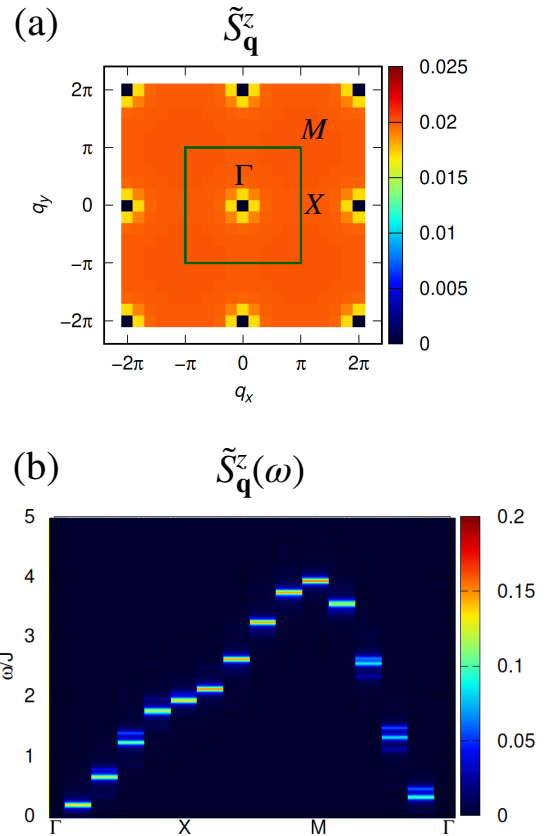


Figure 4: (a) The  $z$ -component of the static spin structure factor  $\tilde{S}_{\mathbf{q}}^z$  and (b) the  $z$ -component of the dynamical spin structure factor  $\tilde{S}_{\mathbf{q}}^z(\omega)$  along the high symmetric momentum line for an  $S=1/2$  isotropic antiferromagnetic Heisenberg model on a square lattice of 100 sites ( $L_x = L_y = 10$ ) with  $N_\downarrow = 2$  near the saturation field. Note that the trivial component in the structure factors is subtracted for visibility (see the text). The high symmetric momenta are indicated by  $\Gamma$ :  $(0, 0)$ ,  $X$ :  $(\pi, 0)$ , and  $M$ :  $(\pi, \pi)$ .

## 5. Summary

We have developed the exact diagonalization package QS<sup>3</sup> for analyzing spin-1/2 quantum lattice models with XXZ interactions near the saturation field. The QS<sup>3</sup> package employs the symmetry-adapted basis sets with respect to the translational symmetry as well as the U(1) symmetry. In order to access large system sizes up to  $O(1000)$ , the QS<sup>3</sup> package does not

use the traditional bit representation for spin configurations. Introducing OpenMP parallelization, the bottleneck of the calculation, i.e., large dimension matrix-vector multiplication, is efficiently accelerated by the parallelization. The QS<sup>3</sup> package computes fundamental physical quantities such as the local magnetization, two-point spin correlation function, and the dynamical spin structure factor. These quantities are essential and observable in experiments. As demonstrated in the benchmark, the QS<sup>3</sup> package can treat three-dimensional systems to understand the ground state as well as the low-energy excitations with potentially interesting properties.

For the future development, the QS<sup>3</sup> package will be extended to treat the point-group symmetry in addition to the translational symmetry. We will also introduce the multiple degrees of freedom per unit cell, i.e., multiple spins per unit cell, to treat more general lattice geometries such as the kagome and pyrochlore lattices. In addition, we will extend the application of the QS<sup>3</sup> packages to dilute fermionis, soft-core bosons, and higher-spin systems. These extensions are straightforward in terms of the coding employed in the QS<sup>3</sup> package and most likely increase a value of the QS<sup>3</sup> package as a research tool not only in condensed matter physics but also in quantum chemistry. For example, the QS<sup>3</sup> package will be able to handle the full configuration interaction (full CI) calculation for molecules with a small number of electrons occupying many orbitals, which are difficult to treat by an available open-source package, e.g., given in Ref. [46].

Furthermore, we can implement a function to simulate quantum circuits with symmetry constraints. This direction of development is important to provide reference data for benchmark results of future large-scale universal quantum computers and to investigate quantum accelerated algorithms for quantum many-body systems. These extensions are in part under progress and will be reported in the near future.

## Acknowledgments

H.U. thanks W. Mizukami for helpful comments. T.S. is supported by the Theory of Quantum Matter Unit of the Okinawa Institute of Science and Technology Graduate University (OIST). The work was partially supported by KAKENHI Nos. 17K14359, 18H01183, 19K14665, 21K03477, and 21H04446, and by JST PRESTO No. JPMJPR1911. This work was also supported by MEXT Q-LEAP Grant Number JPMXS0120319794. We are grateful for allocating computational resources of the HOKUSAI BigWaterfall supercomputing system at RIKEN. The QS<sup>3</sup> package was also developed and performed using the facilities of the Supercomputer Center, ISSP, the University of Tokyo, the facilities of the research center for computational science of national institutes of natural sciences, and the facilities of computing section, OIST.

## References

- [1] E. Dagotto, *Rev. Mod. Phys.* **66**, 763 (1994).
- [2] “MPI Forum,” <https://www.mpi-forum.org/>.
- [3] A. W. Sandvik, *AIP Conference Proceedings* **1297**, 135 (2010).
- [4] “Spin Pack,” <https://www-e.ovgu.de/jschulen/spin/>.
- [5] “Rokko,” <https://github.com/t-sakashita/rokkko>.
- [6] M. Kawamura, K. Yoshimi, T. Misawa, Y. Yamaji, S. Todo, and N. Kawashima, *Computer Physics Communications* **217**, 180 (2017).
- [7] J. Oitmaa and D. D. Betts, *Canadian Journal of Physics* **56**, 897 (1978), <https://doi.org/10.1139/p78-120>.
- [8] P. W. Leung and V. Elser, *Phys. Rev. B* **47**, 5459 (1993).
- [9] C. Waldtmann, H. U. Everts, B. Bernu, C. Lhuillier, P. Sindzingre, P. Lecheminant, and L. Pierre, *The European Physical Journal B - Condensed Matter and Complex Systems* **2**, 501 (1998).
- [10] J. Richter and J. Schulenburg, *The European Physical Journal B* **73**, 117 (2010).
- [11] H. Nakano and T. Sakai, *Journal of the Physical Society of Japan* **79**, 053707 (2010), <https://doi.org/10.1143/JPSJ.79.053707>.
- [12] H. Nakano and T. Sakai, *Journal of the Physical Society of Japan* **80**, 053704 (2011), <https://doi.org/10.1143/JPSJ.80.053704>.
- [13] A. M. Läuchli, J. Sudan, and E. S. Sørensen, *Phys. Rev. B* **83**, 212401 (2011).
- [14] H. Nakano and T. Sakai, *Journal of the Physical Society of Japan* **84**, 063705 (2015), <https://doi.org/10.7566/JPSJ.84.063705>.
- [15] H. Nakano, N. Todoroki, and T. Sakai, *Journal of the Physical Society of Japan* **88**, 114702 (2019), <https://doi.org/10.7566/JPSJ.88.114702>.
- [16] A. M. Läuchli, J. Sudan, and R. Moessner, *Phys. Rev. B* **100**, 155142 (2019).
- [17] C. Lanczos, *J. Res. Natl. Bur. Stand. B* **45**, 255 (1950).
- [18] A. Wietek and A. M. Läuchli, *Phys. Rev. E* **98**, 033309 (2018).
- [19] K. Watanabe, H. Kawamura, H. Nakano, and T. Sakai, *Journal of the Physical Society of Japan* **83**, 034714 (2014), <https://doi.org/10.7566/JPSJ.83.034714>.
- [20] H. Kawamura, K. Watanabe, and T. Shimokawa, *Journal of the Physical Society of Japan* **83**, 103704 (2014), <https://doi.org/10.7566/JPSJ.83.103704>.
- [21] T. Shimokawa, K. Watanabe, and H. Kawamura, *Phys. Rev. B* **92**, 134407 (2015).
- [22] K. Uematsu and H. Kawamura, *Journal of the Physical Society of Japan* **86**, 044704 (2017), <https://doi.org/10.7566/JPSJ.86.044704>.
- [23] K. Uematsu and H. Kawamura, *Phys. Rev. B* **98**, 134427 (2018).
- [24] K. Uematsu and H. Kawamura, *Phys. Rev. Lett.* **123**, 087201 (2019).
- [25] “TITPACK Ver.2,” [http://www.qa.iir.titech.ac.jp/~nishimori/titpack2\\_new/index-e.html](http://www.qa.iir.titech.ac.jp/~nishimori/titpack2_new/index-e.html).
- [26] P. Weinberg and M. Bukov, *SciPost Phys.* **2**, 003 (2017).
- [27] P. Weinberg and M. Bukov, *SciPost Phys.* **7**, 20 (2019).
- [28] When we use standard 32 (64)-bit signed integer, the range is restricted from  $-2^{31(63)}$  to  $2^{31(63)}+1$ .
- [29] D. Yamamoto, H. Ueda, I. Danshita, G. Marmorini, T. Momoi, and T. Shimokawa, *Phys. Rev. B* **96**, 014431 (2017).
- [30] K. Wu, A. Canning, H. Simon, and L.-W. Wang, *Journal of Computational Physics* **154**, 156 (1999).
- [31] K. Wu and H. Simon, *SIAM Journal on Matrix Analysis and Applications* **22**, 602 (2000), <https://doi.org/10.1137/S0895479898334605>.
- [32] E. Anderson, Z. Bai, C. Bischof, S. Blackford, J. Demmel, J. Dongarra, J. Du Croz, A. Greenbaum, S. Hammerling, A. McKenney, *et al.*, *LAPACK Users' Guide: Third Edition*, Software, Environments, and Tools (Society for Industrial and Applied Mathematics, 1999).
- [33] R. Haydock, V. Heine, and M. J. Kelly, *J. Phys. C* **5**, 2845 (1972).
- [34] E. R. Gagliano and C. A. Balseiro, *Phys. Rev. Lett.* **59**, 2999 (1987).
- [35] M. Blume and Y. Y. Hsieh, *Journal of Applied Physics* **40**, 1249 (1969), <https://doi.org/10.1063/1.1657616>.
- [36] A. Andreev and I. A. Grishchuk, *Zh. Eksp. Teor. Fiz.* **87**, 267 (1984).
- [37] N. Shannon, T. Momoi, and P. Sindzingre, *Phys. Rev. Lett.* **96**, 027213 (2006).
- [38] B. Schmidt, P. Thalmeier, and N. Shannon, *Phys. Rev. B* **76**, 125113 (2007).
- [39] L. Kecke, T. Momoi, and A. Furusaki, *Phys. Rev. B* **76**, 060407 (2007).
- [40] T. Hikihara, L. Kecke, T. Momoi, and A. Furusaki, *Phys. Rev. B* **78**, 144404 (2008).
- [41] J. Sudan, A. Läuscher, and A. M. Läuchli, *Phys. Rev. B* **80**, 140402 (2009).
- [42] H. T. Ueda and K. Totsuka, *Phys. Rev. B* **80**, 014417 (2009).
- [43] M. Sato, T. Hikihara, and T. Momoi, *Phys. Rev. Lett.* **110**, 077206 (2013).
- [44] H. T. Ueda and T. Momoi, *Phys. Rev. B* **87**, 144417 (2013).
- [45] H. T. Ueda, *Journal of the Physical Society of Japan* **84**, 023601 (2015).

<https://doi.org/10.7556/JPSJ.84.023601> .

- [46] K. D. Vogiatzis, D. Ma, J. Olsen, L. Gagliardi, and W. A. de Jong, *The Journal of Chemical Physics* **147**, 184111 (2017).